catalysts

MDPI

Article

Interface Engineering-Induced 1T-MoS_2/NiS Heterostructure for Efficient Hydrogen Evolution Reaction

Helei Wei [1,†], Aidong Tan [1,2,†], Wenbo Liu [1], Jinhua Piao [3], Kai Wan [1,*], Zhenxing Liang [1], Zhipeng Xiang [1,*] and Zhiyong Fu [1,*]

[1] Guangdong Provincial Key Laboratory of Fuel Cell Technology, School of Chemistry and Chemical Engineering, South China University of Technology, Guangzhou 510641, China
[2] Institute of Energy Power Innovation, North China Electric Power University, Beijing 102206, China
[3] School of Food Science and Engineering, South China University of Technology, Guangzhou 510641, China
* Correspondence: wank@scut.edu.cn (K.W.); xzp20209094@scut.edu.cn (Z.X.); zyfu@scut.edu.cn (Z.F.)
† The authors contributed equally to this work.

Abstract: Metal phase molybdenum disulfide (1T-MoS_2) is considered a promising electrocatalyst for the hydrogen evolution reaction (HER). In this work, an interface engineering-induced strategy is reported to prepare a 1T-MoS_2/NiS heterostructure. The 1T-MoS_2/NiS heterostructure exhibits an enhanced HER activity compared with that of the 1T-MoS_2 in 1.0 M KOH. It achieves an overpotential of 0.12 V at a current density of 10 mA cm^{-2} with a Tafel slope of 69 mV dec^{-1}. The density functional theory (DFT) calculations reveal that the interface engineering-induced 1T-MoS_2/NiS heterostructure exhibits regulated electronic states of the S sites in 1T-MoS_2, thus promoting the HER activity. This work demonstrates that tuning the electronic structure through interface engineering to enhance the intrinsic activity of electrocatalysts is a feasible strategy.

Keywords: interface engineering; heterostructure; 1T-MoS_2/NiS; hydrogen evolution reaction

check for updates

Citation: Wei, H.; Tan, A.; Liu, W.; Piao, J.; Wan, K.; Liang, Z.; Xiang, Z.; Fu, Z. Interface Engineering-Induced 1T-MoS_2/NiS Heterostructure for Efficient Hydrogen Evolution Reaction. *Catalysts* **2022**, *12*, 947. https://doi.org/10.3390/catal12090947

Academic Editors: Dezhi Han, Wentai Wang and Ning Han

Received: 2 August 2022
Accepted: 22 August 2022
Published: 25 August 2022

1. Introduction

Molybdenum disulfide (MoS_2) is regarded as a promising electrocatalyst for the hydrogen evolution reaction (HER) due to its abundant edge sites [1–5]. However, the catalytic performance is not as expected in practical applications. In the past years, enormous efforts have been devoted to fabricating various MoS_2 electrocatalysts to improve the HER activity, such as adjusting the size [6], regulating the layer number [7,8], heteroatom doping [9], creating vacancies [10], phase engineering [11] and interface engineering [12–14]. The 1T phase MoS_2 (octahedral structure) catalysts have attracted significant attention because of the dense active sites on their basal plane and edge site [15]. The metallic 1T-MoS_2 exhibits a conductivity that is about six orders of magnitudes higher than that of the semiconductor 2H-MoS_2, which ensures a fast charge transfer during the electrode reaction [16]. However, 1T-MoS_2 is thermodynamically metastable, which can spontaneously transform into 2H-MoS_2 at a certain temperature [17]. The traditional synthesis methods of 1T-MoS_2 always involve harsh conditions and a complex process, such as the alkali metal intercalation or exfoliation process, making it difficult to synthesize in batches [18].

In recent years, hybrid materials, which feature heterostructures, have attracted much attention due to their decent HER electrocatalysis activity. The catalysts, such as Ni_3S_2@MoS_2 [19], 1T-MoS_2/NiS_2 [20], MoS_2/NiS [21], MoS_2/NiS nanoflowers [22], etc., have been explored. Notably, the interface engineering-induced strategy has been developed to prepare the 1T-MoS_2, which possesses easy operation, a low energy consumption and high conversion rate [20,23]. Theoretical and experimental studies revealed that interface engineering can trigger the slip of S atoms, thus transforming the 2H to the 1T phase [24]. For example, Park et al. reported an edge-aligned 2H-MoS_2 and reduced

graphene oxide heterointerface-induced interface charge transfer, resulting in a phase conversion of 2H-MoS_2 to 1T-MoS_2 [17]. Moreover, the obtained heterostructure can regulate the electronic structure of the 1T-MoS_2, thus improving the intrinsic electrocatalytic activity of HER. Song et al. reported a 1T-MoS_2/CoS_2 heterostructure by an interface engineering-induced in situ growth with molybdate cobalt oxide nanowire as a precursor and thiourea as a sulfur source [25]. The obtained MoS_2/CoS_2 heterostructure yields a regulated electronic structure at the interface, thus achieving a near zero Gibbs free energy for hydrogen adsorption. Therefore, it is plausible to develop an interface engineering-induced strategy to fabricate highly conductive 1T-MoS_2 with a modulated electronic structure at its interface to boost the HER.

In line with the above understanding, a two-dimensional 1T-MoS_2/NiS heterostructure was prepared by an interface engineering-induced strategy to boost the HER in alkaline media. The physiochemical characterizations reveal that the obtained 1T-MoS_2/NiS features a typical heterostructure with interlinked 1T-MoS_2 and NiS. The 1T-MoS_2/NiS heterostructure shows a strong electronic interaction between 1T-MoS_2 and NiS. Density functional theory (DFT) calculations reveal that the electrons were transferred from Ni to the adjacent S in 1T-MoS_2, thus facilitating the chemical adsorption step of the HER. The electrochemical results confirm that the 1T-MoS_2/NiS heterostructure exhibits an improved HER electrocatalytic activity compared with that of the 1T-MoS_2.

2. Results and Discussion

2.1. Material Synthesis and Characterization

The 1T-MoS_2/NiS heterostructure is synthesized by an interface engineering-induced strategy with a two-dimensional Ni nanosheet (Figure S1) as the substrate, as illustrated in Scheme 1. First, the Ni nanosheets are dispersed in a mixed solution of ethanol and deionized water with MoO_3 as a Mo precursor and KSCN as a sulfur source. Then, the above solution is subjected to a solvothermal treatment at 180 °C for 24 h to obtain the 1T-MoS_2/NiS heterostructure. The possible growth mechanism is as follows: Under the high-temperature and high-pressure conditions, the active metallic Ni is easily oxidized to Ni^{2+} and reacts with the sulfur source to form NiS at the initial stage. Then, the NiS serves as the substrate to form composite structures [26]. The MoO_3 (Mo VI) is slowly reduced to Mo (IV) in the presence of ethanol, and the resultant Mo (IV) reacts with SCN^- to produce MoS_2 on the NiS surface to form heterostructures [21,27].

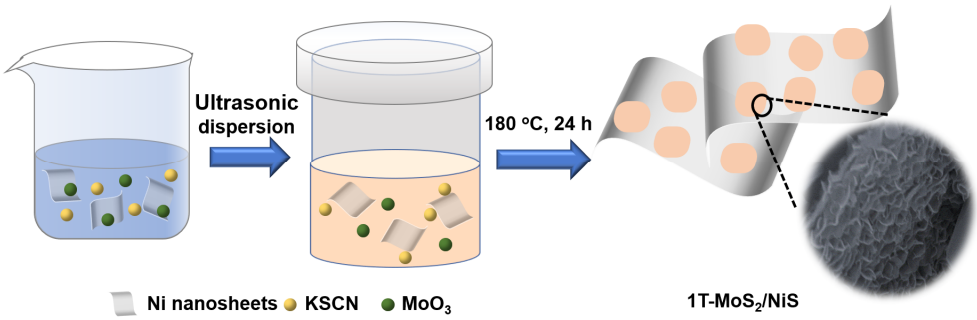

Scheme 1. Schematic illustration of the synthesis process.

The scanning/transmission electron microscopy (SEM/TEM) is employed to characterize the microscopic morphology of the synthesized materials (Figure 1a,b). It is seen that the 1T-MoS_2/NiS heterostructure shows a distinct nanosheet-like morphology. Scanning transmission electron microscopy–energy dispersive X-ray (STEM-EDX) element mapping results confirm the presence of Ni, Mo and S elements and the uniform distribution (Figure 1c). The high-resolution TEM (HRTEM) image shows well-resolved lattice fringes with a d-spacing of 0.278 nm, which correspond to the (300) lattice plane of NiS (Figure 1d). Remarkably, the region marked with yellow corresponds to the crystal structure of 1T phase MoS_2 (Figure 1e,f) [28,29]. The above results suggest the successful fabrication of

the 1T-MoS_2/NiS heterostructure by the interface engineering-induced strategy [25]. In comparison, the 2H-MoS_2 is prepared without the presence of the Ni nanosheet, which also exhibits a nanosheet-like morphology as the 1T-MoS_2/NiS heterostructure (Figure S2). The above results suggest that the Ni nanosheet plays a significant role in inducing the formation of the 1T-MoS_2 phase.

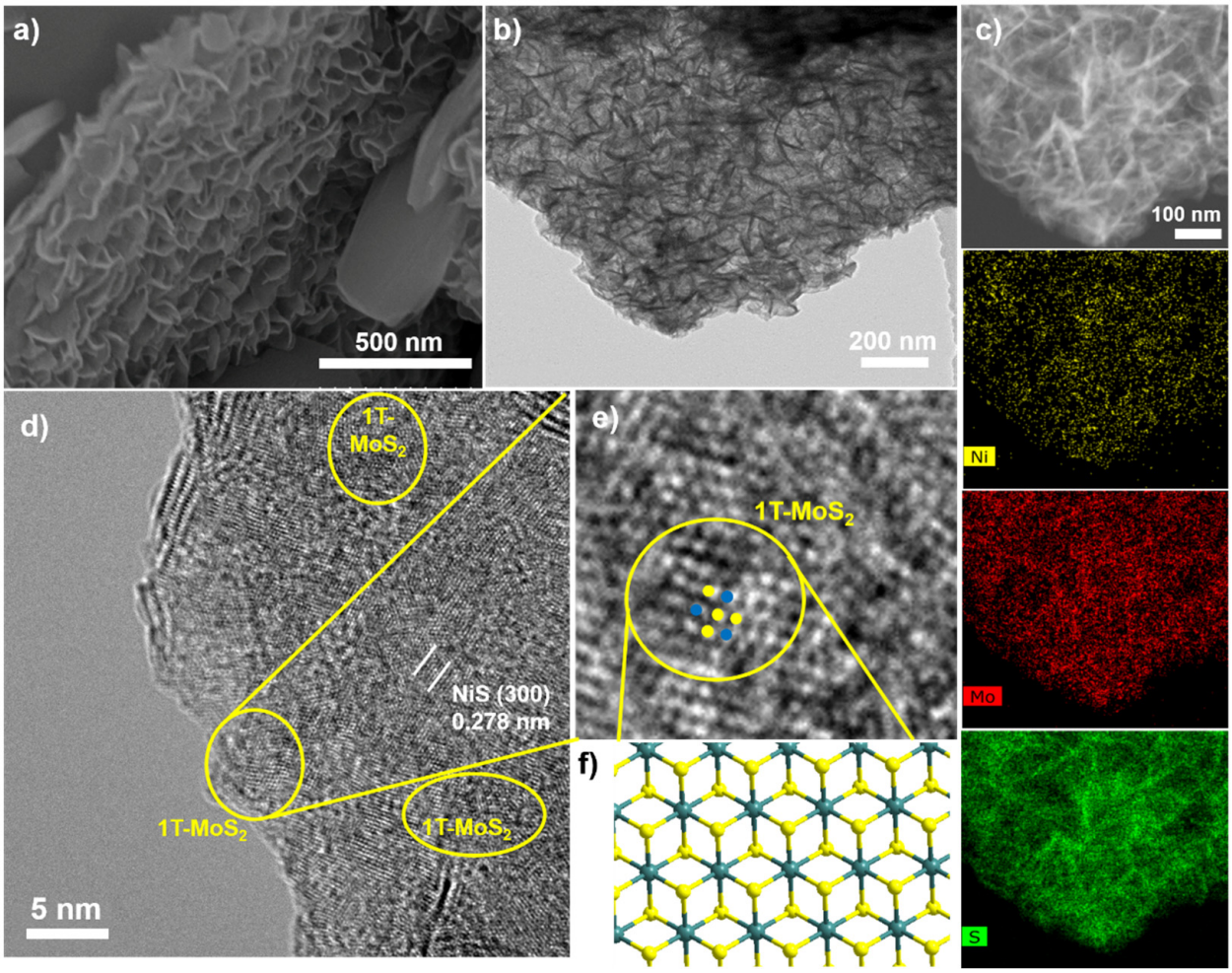

Figure 1. (**a**) SEM image, (**b**) TEM image and (**c**) STEM-EDX elemental mapping of the 1T-MoS_2/NiS; (**d**) HRTEM image on the basal plane of 1T-MoS_2/NiS and (**e**,**f**) zoom-in view of the selected regions and the lattice schematic of 1T-MoS_2.

X-ray diffraction (XRD) is used to identify the crystal structure of the prepared catalysts (Figure 2a). As shown in Figure 2a, the diffraction peaks at 14.1°, 32.9° and 58.8° correspond to the (002), (100) and (110) planes of the MoS_2 (PDF#75-1539) for both 1T-MoS_2 and 2H-MoS_2, respectively. In addition, the broadened diffraction peaks suggest a low crystallinity of the MoS_2 electrocatalysts. While the diffraction peaks of 1T-MoS_2/NiS at 18.4°, 30.3°, 32.2°, 35.7°, 40.4° and 48.8° are matched well with (111), (101), (300), (021), (211) and (131) planes of hexagonal phase NiS (PDF#12-0041), respectively, it is worth noting that no obvious peak of 1T-MoS_2 was detected in the 1T-MoS_2/NiS heterostructure, which may be due to its relatively low crystallinity compared with the high crystallinity NiS [30].

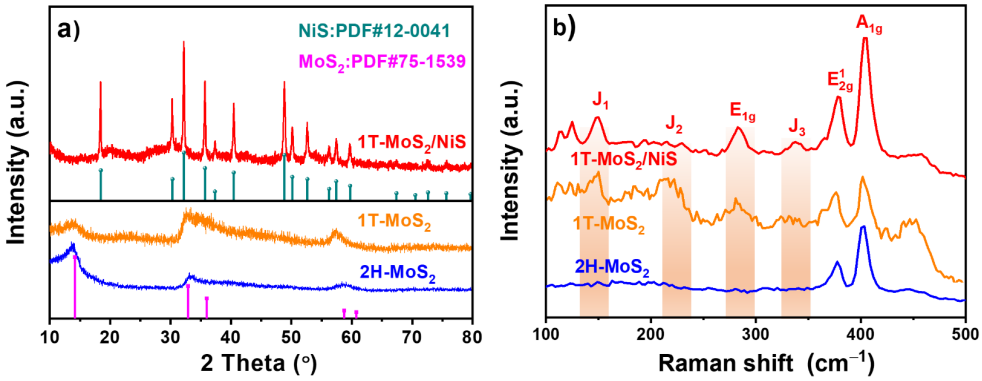

Figure 2. (**a**) XRD spectra and (**b**) Raman spectra of the 2H-MoS_2, 1T-MoS_2 and 1T-MoS_2/NiS.

The Raman spectroscopy is further used to confirm the crystal structure of the 1T-MoS_2/NiS heterostructure. A crucial difference between 2H-MoS_2 and 1T-MoS_2 is the symmetry of the S atoms in their structures. It is seen that the 2H-MoS_2 exhibits two main characteristic peaks of E^1_{2g} (383 cm^{-1}) and A_{1g} (408 cm^{-1}). The E^1_{2g} peak involves the molecular vibrations mode of Mo and S atoms in the 2g layer, while the A_{1g} peak involves the molecular vibration mode of S atom symmetry outside the layer along the c-axis [31]. For the 1T-MoS_2 and 1T-MoS_2/NiS heterostructure, there are four new characteristic peaks that can be observed at J_1 (147 cm^{-1}), J_2 (236 cm^{-1}), E_{1g} (283 cm^{-1}) and J_3 (335 cm^{-1}), confirming the existence of 1T phase MoS_2 [32]. This result further confirms that the interface engineering induced the formation of the 1T-MoS_2 phase.

The elemental composition and chemical states are determined by X-ray photoelectron spectroscopy (XPS), as shown in Figure 3. The XPS survey spectra of 1T-MoS_2 and 1T-MoS_2/NiS show the signals of Mo, S, O and C (Figure 3a). The presence of O may be attributed to the surface oxidation of the materials, while C originated from the carbon substrate. In the 1T-MoS_2/NiS heterostructure, the Ni is detected and the atomic ratio of Mo to Ni is around 3:1. It is seen that the peaks around 228.6 and 231.9 eV correspond to the Mo $3d_{3/2}$ and Mo $3d_{5/2}$, respectively (Figure 3b). It is seen that the Mo $3d_{3/2}$ and Mo $3d_{5/2}$ of 1T-MoS_2/NiS shift to lower binding energies than that of the 1T-MoS_2, indicating a strong electronic interaction between the 1T-MoS_2 and the NiS species in the 1T-MoS_2/NiS heterostructure [33]. Similarly, the S 2p peak of 1T-MoS_2/NiS also shifts to lower binding energies than that of the 1T-MoS_2 (Figure 3c). The detailed XPS analysis of the Mo 3d, Ni 2p and S 2p are shown in Figure 3d–f. It is seen that the high-resolution Mo 3d spectrum of the 1T-MoS_2/NiS is mainly deconvoluted into four peaks of Mo $3d_{5/2}$, Mo $3d_{3/2}$, S 2s and Mo^{6+} (Figure 3d). The two characteristic peaks of Mo $3d_{5/2}$ (228.3 eV) and Mo $3d_{3/2}$ (231.3 eV) correspond to the production of Mo^{4+} in 1T-MoS_2/NiS [20]. The peaks located at around 229.5 eV and 232.4 eV can be attributed to the Mo^{4+} in the 2H phase, which is ~1.1 eV higher than the corresponding peaks in 1T-MoS_2 (red line) [34]. Based on the analysis and discussion of the high-resolution Mo 3d spectra and the fitting results [35], it is worth noting that the relative content of the 1T phase (red line) in the catalyst is estimated to be ~38.9%, and the 1T/2H phase ratio was determined to be 0.64. The peak at ~225.9 eV can be allocated to S 2s [30], Moreover, the peaks located at 234.3 eV and 235.6 eV correspond to Mo^{6+}, which possibly arises from the surface oxidation of Mo^{4+} when exposed to air [36]. The high-resolution Ni 2p spectrum of the 1T-MoS_2/NiS is deconvoluted into four peaks of Ni $2p_{1/2}$ (874.4 eV), Ni $2p_{3/2}$ (856.5 eV) and two satellite peaks (861.3 and 879.4 eV) (Figure 3e), which correspond to the characteristics peaks of Ni^{2+} [19]. In the S 2p spectrum (Figure 3f), the peak at 164.3 eV is associated with bridging disulfides S_2^{2-}, implying the unsaturated S atoms on NiS and MoS sites [37,38]. The peak at 161.1 eV (S $2p_{3/2}$) and 162.5 eV (S $2p_{1/2}$) is consistent with S^{2-} species in 1T-MoS_2 [39,40].

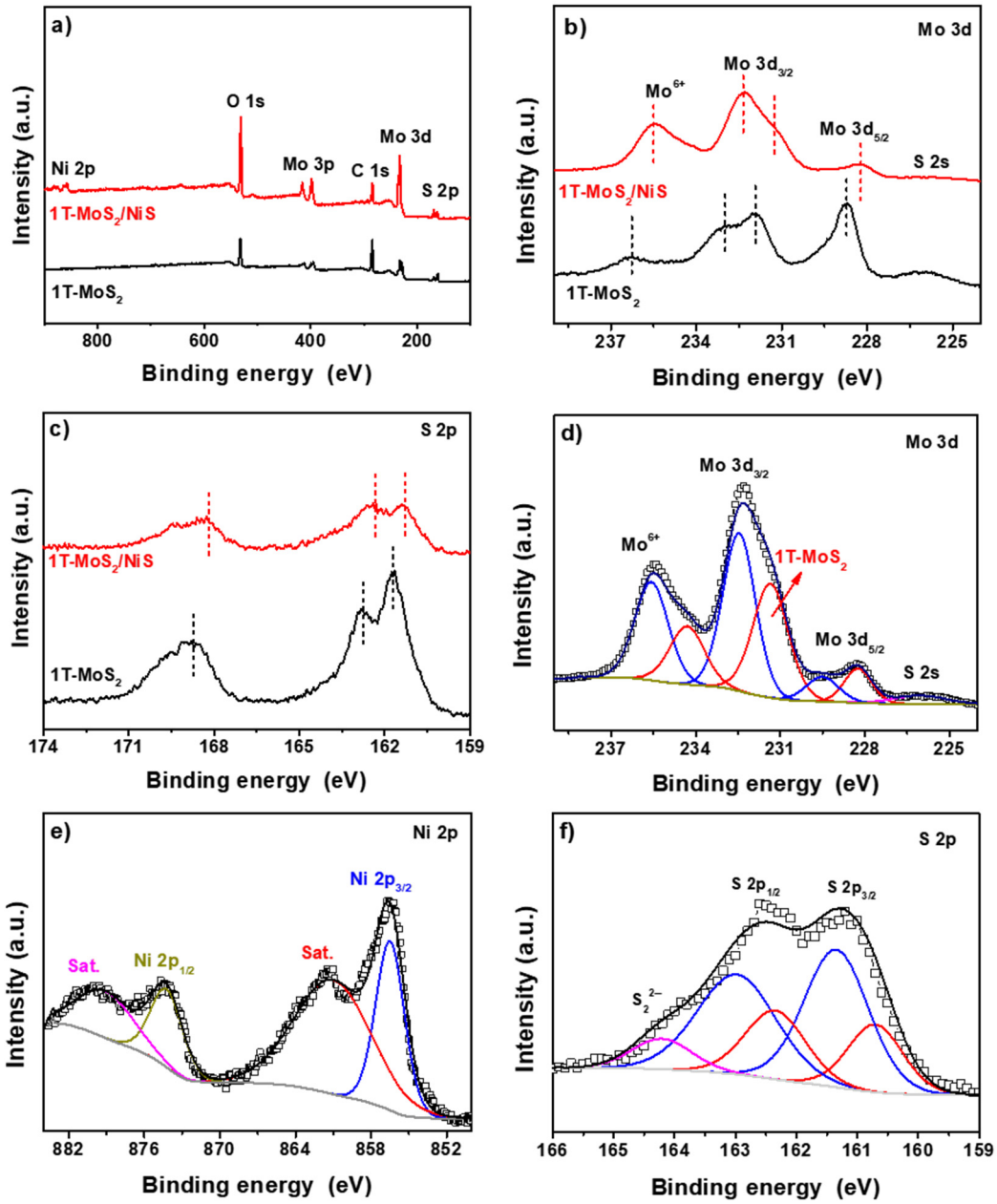

Figure 3. (**a**) XPS survey spectra of 1T-MoS_2 and 1T-MoS_2/NiS; high-resolution peaks of (**b**) Mo 3d and (**c**) S 2p of 1T-MoS_2 and 1T-MoS_2/NiS; high-resolution peaks and fitting results of 1T-MoS_2/NiS: (**d**) Mo 3d, (**e**) Ni 2p and (**f**) S 2p.

2.2. Electrochemical Activity

Electrocatalytic activity of the as-prepared 1T-MoS_2/NiS heterostructure towards the HER is evaluated in 1.0 M KOH. For comparison, the HER electrocatalytic activity of the Ni-doped MoS_2 (Ni-MoS_2), 1T-MoS_2, 2H-MoS_2 and NiS are also examined under the same conditions. As shown in Figure 4a,b, carbon fiber paper (CFP) exhibits negligible HER activity compared to the obtained electrocatalysts. It is seen that the 1T-MoS_2 shows a much lower overpotential of 0.19 V than that of the 2H-MoS_2 (0.29 V) at the current density of 10 mA cm^{-2} (Figure 4a,b), which may be attributed to its increased conductivity and active sites. It is reported that the 1T-MoS_2 exhibits an inherent conductivity, thus promoting the charge transfer of HER, and both the basal plane and edge are active sites [41]. Among the electrocatalysts, the 1T-MoS_2/NiS heterostructure shows the lowest overpotential of 0.12 V at the current density of 10 mA cm^{-2}, which is lower than that of

1T-MoS_2. In particular, this trend is still maintained at a high current density of 100 mA cm^{-2}, and the results are summarized in Figure 4b. Moreover, 1T-MoS_2/NiS shows a much higher overpotential than that of the commercial Pt/C electrocatalyst (0.03 V) at a current density of 10 mA cm^{-2}, while attaining comparable performance at high current densities (100 mA cm^{-2}) (Figure S3).

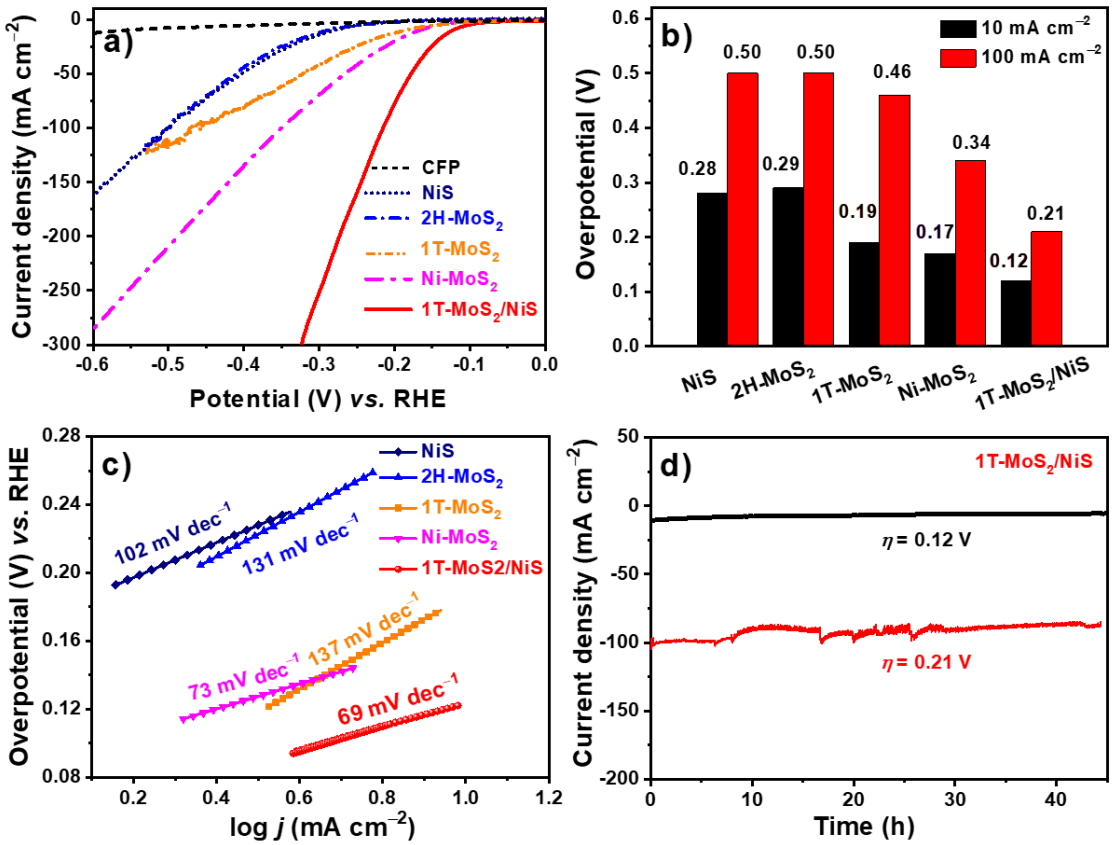

Figure 4. The electrochemical characterization of all electrocatalysts in 1.0 M KOH. (**a**) Polarization curves (without *iR* correction) and corresponding (**b**) overpotential at a current density of 10 mA cm^{-2} and 100 mA cm^{-2} and (**c**) Tafel plots; (**d**) durability tests of the 1T-MoS_2/NiS catalyst at a constant potential of −0.12 V and −0.21 V vs. RHE.

To further evaluate the HER kinetics of the catalysts, the Tafel slopes are obtained by linearly fitting the polarization curves of HER based on the Tafel equation [42–44]. As shown in Figure 4c, the 1T-MoS_2/NiS heterostructure shows the lowest Tafel slope compared with the other prepared electrocatalysts, indicating the fastest kinetic of 1T-MoS_2/NiS (Figure 4c). The Tafel slope of the 1T-MoS_2/NiS is 69 mV dec^{-1}, indicating the Volmer–Heyrovsky mechanism of the HER pathway [45,46]. The electrochemical impedance spectroscopy (EIS) is also employed to study the charge transfer resistance (R_{ct}) of the electrocatalysts. It is seen that the 1T-MoS_2/NiS exhibits a charge transfer resistance of ~0.4 Ω, which is much lower than that of 1T-MoS_2 (~ 2.9 Ω) (Figure S4). This result indicates that the strong interaction between NiS and 1T-MoS_2 can significantly facilitate charge transfer. The detailed mechanism analysis of the electrocatalytic activity enhancement is further explored by the density functional theory (DFT) calculations (see below).

Finally, the stability of the as-prepared 1T-MoS_2/NiS is evaluated by chronoamperometry, as shown in Figure 4d. It is seen that the 1T-MoS_2/NiS exhibits good stability with a slight degradation at an overpotential of −0.12 V. It is worth noting that the long stable performance is maintained even at high current densities (black line), the degradation of which we attribute to the partial shedding of the catalyst. As shown in Figure S7 and Table S1, the prepared 1T-MoS_2/NiS heterostructure is equipped with low overpotential

and a small Tafel slope, which indicate the merits of high intrinsic activity and fast HER kinetics, making the 1T-MoS_2/NiS heterostructure one of the promising molybdenum-based sulfide electrocatalysts.

2.3. Mechanism Analysis of the Electrocatalytic Activity Enhancement

To further investigate the reason for the enhanced HER activity of 1T-MoS_2/NiS, the DFT calculations and electronic structure analysis are performed on CP2K 8.1 package. The models of 1T-MoS_2 and 1T-MoS_2/NiS are constructed based on the HRTEM results (Figure 1d,e), as shown in Figures S5 and S6. The electronic structure is investigated to understand the effect of interface engineering. As displayed in Figure 5a, the location of the S orbital relative to the Fermi energy level in 1T-MoS_2/NiS is higher than the counterpart of 1T-MoS_2. The location of S orbital shifts to the Fermi level, resulting in a decreased binding energy [47], which is consistent with the XPS analysis (Figure 3c). As previously reported, the H adsorption on the S site of 1T-MoS_2 is weak, the S orbital shifts to the Fermi level can strengthen the adsorption free energy of H, thus promoting the chemical adsorption step of the HER [48]. The charge density difference map of the 1T-MoS_2/NiS heterostructure exhibits a strong electronic interaction between the 1T-MoS_2 and NiS, in which the electrons are transferred from Ni to the adjacent S in 1T-MoS_2 (Figure 5b). These results suggest that the introduced NiS species regulate the electronic states of S in 1T-MoS_2, thus modifying the adsorption free energy of hydrogen, and finally enhancing the HER activity.

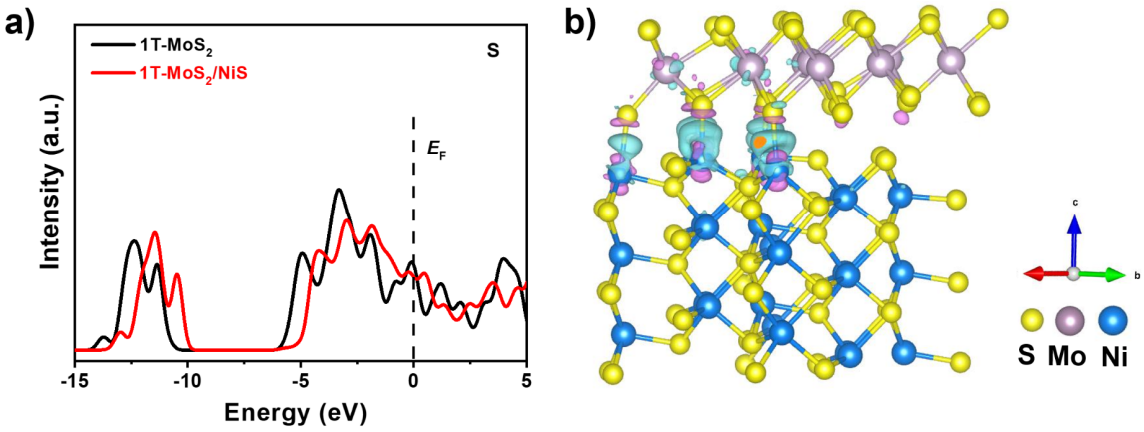

Figure 5. (**a**) Projected density of states (PDOS) of catalysts with the Fermi level set to zero. (**b**) the side view of the charge density distribution of 1T-MoS_2/NiS, showing electron transfer from NiS to 1T-MoS_2, with cyan and pink exhibiting the increase and decrease in electron density, respectively.

3. Conclusions

A novel 1T-MoS_2/NiS nanosheet heterostructure was developed for the HER by an interface engineering-induced strategy. The obtained 1T-MoS_2/NiS electrocatalyst exhibited an enhanced HER activity compared with that of 1T-MoS_2. DFT calculations revealed that the obtained 1T-MoS_2/NiS heterostructure can modulate the electronic structure of S by increasing its electronic density states and shifting towards the Fermi level. The S orbital shifts to the Fermi level can facilitate the chemical adsorption step of the HER, thus enhancing the HER activity. This work may provide fundamental insights and strategies for the rational design of efficient HER electrocatalysts by manipulating the electronic structure.

Supplementary Materials: The following supporting information can be downloaded at: https://www.mdpi.com/article/10.3390/catal12090947/s1, Experimental section; Figure S1: (a) SEM image, (b) TEM image and (c) XRD pattern of the Ni nanosheets, (d) AFM image and (e–f) corresponding thicknesses, Figure S2: (a) SEM image, (b) TEM image and (c) HRTEM image of the 2H-MoS2, (d) crystal structure of 2H-MoS2 nanosheets, Figure S3: (a) Polarization curves (without iR correction) of 1T-MoS2/NiS and commercial Pt/C, Figure S4: Nyquist plots of 1T-MoS2/NiS and 1T-MoS2 (inset is an enlarged view of 1T-MoS2/NiS), Figure S5: Side and top views of the optimized slab models

of 1T-MoS2, Figure S6: Side view and top view of the optimized plate model of the 1T-MoS2/NiS, Figure S7: Performance comparison chart between different materials, Table S1: Comparisons of HER performance of the recently reported MoS_2-based electrocatalysts in 1.0 M KOH. References [49–64] are cited in the supplementary materials.

Author Contributions: Conceptualization, H.W., K.W., Z.X. and A.T.; methodology and writing—original draft preparation, H.W., K.W., Z.X. and A.T.; writing—review and editing, H.W., K.W., W.L., J.P., Z.X., Z.F. and Z.L.; supervision, Z.X., Z.F. and Z.L. All authors have read and agreed to the published version of the manuscript.

Funding: This research was funded by the National Natural Science Foundation of China (Nos. 21903026, 21975081, 21975079, 22178126, 22108085), China Postdoctoral Science Foundation (2022M711196).

Data Availability Statement: Data sharing is not applicable to this article.

Conflicts of Interest: The authors declare no conflict of interest.

References

1. Wang, H.; Xiao, X.; Liu, S.; Chiang, C.L.; Kuai, X.; Peng, C.K.; Lin, Y.C.; Meng, X.; Zhao, J.; Choi, J.; et al. Structural and Electronic Optimization of MoS_2 Edges for Hydrogen Evolution. *J. Am. Chem. Soc.* **2019**, *141*, 18578–18584. [CrossRef] [PubMed]
2. Yang, L.; Liu, P.; Li, J.; Xiang, B. Two-Dimensional Material Molybdenum Disulfides as Electrocatalysts for Hydrogen Evolution. *Catalysts* **2017**, *7*, 285. [CrossRef]
3. Tsai, C.; Li, H.; Park, S.; Park, J.; Han, H.S.; Norskov, J.K.; Zheng, X.; Abild Pedersen, F. Electrochemical Generation of Sulfur Vacancies in the Basal Plane of MoS_2 for Hydrogen Evolution. *Nat. Commun.* **2017**, *8*, 15113. [CrossRef] [PubMed]
4. Tang, T.; Wang, Z.; Guan, J. A Review of Defect Engineering in Two-Dimensional Materials for Electrocatalytic Hydrogen Evolution Reaction. *Chin. J. Catal.* **2022**, *43*, 636–678. [CrossRef]
5. Wan, K.; Xiang, Z.; Liu, W.; Wei, H.; Fu, Z.; Liang, Z. Recent Progress of Transition Metal Sulfides as Electrocatalysts for Hydrogen/Oxygen Evolution Reactions. *Chin. Sci. Bull.* **2022**, *67*, 2126–2141. [CrossRef]
6. An, Y.R.; Fan, X.L.; Luo, Z.F.; Lau, W.M. Nanopolygons of Monolayer MS_2: Best Morphology and Size for HER Catalysis. *Nano Lett.* **2017**, *17*, 368–376.
7. Li, Y.; Zhang, R.; Zhou, W.; Wu, X.; Zhang, H.; Zhang, J. Hierarchical MoS_2 Hollow Architectures with Abundant Mo Vacancies for Efficient Sodium Storage. *ACS Nano* **2019**, *13*, 5533–5540. [CrossRef]
8. Hua, S.; Qu, D.; An, L.; Xi, G.; Chen, G.; Li, F.; Zhou, Z.; Sun, Z. Highly Dispersed Few-Layer MoS_2 Nanosheets on S, N Co-Doped Carbon for Electrocatalytic H_2 Production. *Chin. J. Catal.* **2017**, *38*, 1028–1037.
9. Aliaga, J.; Vera, P.; Araya, J.; Ballesteros, L.; Urzua, J.; Farias, M.; Paraguay-Delgado, F.; Alonso-Nunez, G.; Gonzalez, G.; Benavente, E. Electrochemical Hydrogen Evolution over Hydrothermally Synthesized Re-Doped MoS_2 Flower-Like Microspheres. *Molecules* **2019**, *24*, 4631.
10. Yang, Q.; Wang, Z.; Dong, L.; Zhao, W.; Jin, Y.; Fang, L.; Hu, B.; Dong, M. Activating MoS_2 with Super-High Nitrogen-Doping Concentration as Efficient Catalyst for Hydrogen Evolution Reaction. *J. Phys. Chem. C* **2019**, *123*, 10917–10925.
11. Li, H.; Chen, S.; Jia, X.; Xu, B.; Lin, H.; Yang, H.; Song, L.; Wang, X. Amorphous Nickel-Cobalt Complexes Hybridized with 1T-Phase Molybdenum Disulfide via Hydrazine-Induced Phase Transformation for Water Splitting. *Nat. Commun.* **2017**, *8*, 15377. [CrossRef] [PubMed]
12. Cheng, P.F.; Feng, T.; Liu, Z.W.; Wu, D.Y.; Yang, J. Laser-Direct-Writing of 3D Self-Supported NiS_2/MoS_2 Heterostructures as an Efficient Electrocatalyst for Hydrogen Evolution Reaction in Alkaline and Neutral Electrolytes. *Chin. J. Catal.* **2019**, *40*, 1147–1152. [CrossRef]
13. Liu, X.; Wang, C. In Situ Wet Etching of MoS_2@dWO_3 Heterostructure as Ultra-Stable Highly Active Electrocatalyst for Hydrogen Evolution Reaction. *Catalysts* **2020**, *10*, 977. [CrossRef]
14. Choi, H.; Lee, S.; Kim, M.C.; Park, Y.; Jang, A.R.; Ahn, W.; Sohn, J.I.; Park, J.B.; Hong, J.; Lee, Y.W. Hierarchically Ordinated Two-Dimensional MoS_2 Nanosheets on Three-Dimensional Reduced Graphene Oxide Aerogels as Highly Active and Stable Catalysts for Hydrogen Evolution Reaction. *Catalysts* **2021**, *11*, 182. [CrossRef]
15. Voiry, D.; Salehi, M.; Silva, R.; Fujita, T.; Chen, M.; Asefa, T.; Shenoy, V.B.; Eda, G.; Chhowalla, M. Conducting MoS_2 Nanosheets as Catalysts for Hydrogen Evolution Reaction. *Nano Lett.* **2013**, *13*, 6222–6227. [CrossRef]
16. Eda, G.; Yamaguchi, H.; Voiry, D.; Fujita, T.; Chen, M.; Chhowalla, M. Photoluminescence from Chemically Exfoliated MoS_2. *Nano Lett.* **2011**, *11*, 5111–5116. [CrossRef]
17. Zhang, K.; Jin, B.; Gao, Y.; Zhang, S.; Shin, H.; Zeng, H.; Park, J.H. Aligned Heterointerface-Induced 1T-MoS_2 Monolayer with Near-Ideal Gibbs Free for Stable Hydrogen Evolution Reaction. *Small* **2019**, *15*, 1804903. [CrossRef]
18. Lukowski, M.A.; Daniel, A.S.; Meng, F.; Forticaux, A.; Li, L.; Jin, S. Enhanced Hydrogen Evolution Catalysis from Chemically Exfoliated Metallic MoS_2 Nanosheets. *J. Am. Chem. Soc.* **2013**, *135*, 10274–10277. [CrossRef]

19. Cui, B.; Zhang, M.; Zhao, Y.; Hu, S. Heterogenization of Few-Layer MoS_2 with Highly Crystalline 3D Ni_3S_2 Nanoframes Effectively Synergizes the Electrocatalytic Hydrogen Generation in Alkaline Medium. *Mater. Today Energy* **2019**, *13*, 85–92. [CrossRef]
20. Chen, X.; Wang, Z.; Wei, Y.; Zhang, X.; Zhang, Q.; Gu, L.; Zhang, L.; Yang, N.; Yu, R. High Phase-Purity 1T-MoS_2 Ultrathin Nanosheets by a Spatially Confined Template. *Angew. Chem. Int. Ed.* **2019**, *58*, 17621–17624. [CrossRef]
21. Qin, Q.; Chen, L.; Wei, T.; Liu, X. MoS_2/NiS Yolk-Shell Microsphere-Based Electrodes for Overall Water Splitting and Asymmetric Supercapacitor. *Small* **2018**, *15*, 1803639. [CrossRef] [PubMed]
22. Zhao, X.; Bao, J.; Zhou, Y.; Zhang, Y.; Sheng, X.; Wu, B.; Wang, Y.; Zuo, C.; Bu, X. Heterostructural MoS_2/NiS Nanoflowers Via Precise Interface Modification for Enhancing Electrocatalytic Hydrogen Evolution. *New J. Chem.* **2022**, *46*, 5505–5514. [CrossRef]
23. Liu, Z.; Wang, K.; Li, Y.; Yuan, S.; Huang, G.; Li, X.; Li, N. Activation Engineering on Metallic 1T-MoS_2 by Constructing In-Plane Heterostructure for Efficient Hydrogen Generation. *Appl. Catal. B Environ.* **2022**, *300*, 120696. [CrossRef]
24. Liu, Q.; Fang, Q.; Chu, W.; Wan, Y.; Li, X.; Xu, W.; Habib, M.; Tao, S.; Zhou, Y.; Liu, D.; et al. Electron-Doped 1T-MoS_2 via Interface Engineering for Enhanced Electrocatalytic Hydrogen Evolution. *Chem. Mater.* **2017**, *29*, 4738–4744. [CrossRef]
25. Feng, Y.; Zhang, T.; Zhang, J.; Fan, H.; He, C.; Song, J. 3D 1T-MoS_2/CoS_2 Heterostructure via Interface Engineering for Ultrafast Hydrogen Evolution Reaction. *Small* **2020**, *16*, 2002850. [CrossRef]
26. Wang, X.; Li, L.; Wang, Z.; Tan, L.; Wu, Z.; Liu, Z.; Gai, S.; Yang, P. NiS_2/MoS_2 on Carbon Cloth as a Bifunctional Electrocatalyst for Overall Water Splitting. *Electrochim. Acta* **2019**, *326*, 134983. [CrossRef]
27. Tian, Y.; He, Y.; Zhu, Y. Low Temperature Synthesis and Characterization of Molybdenum Disulfide Nanotubes and Nanorods. *Mater. Chem. Phys.* **2004**, *87*, 87–90. [CrossRef]
28. Du, Z.; Yang, S.; Li, S.; Lou, J.; Zhang, S.; Wang, S.; Li, B.; Gong, Y.; Song, L.; Zou, X.; et al. Conversion of Non-Van Der Waals Solids to 2D Transition-Metal Chalcogenides. *Nature* **2020**, *577*, 492–496. [CrossRef]
29. Acerce, M.; Voiry, D.; Chhowalla, M. Metallic 1T Phase MoS_2 Nanosheets as Supercapacitor Electrode Materials. *Nat. Nanotechnol.* **2015**, *10*, 313–318. [CrossRef]
30. Shah, S.A.; Shen, X.; Xie, M.; Zhu, G.; Ji, Z.; Zhou, H.; Xu, K.; Yue, X.; Yuan, A.; Zhu, J.; et al. Nickel@Nitrogen-Doped Carbon@MoS_2 Nanosheets: An Efficient Electrocatalyst for Hydrogen Evolution Reaction. *Small* **2019**, *15*, 1804545. [CrossRef]
31. Shi, Y.; Zhou, Y.; Yang, D.R.; Xu, W.X.; Wang, C.; Wang, F.B.; Xu, J.J.; Xia, X.H.; Chen, H.Y. Energy Level Engineering of MoS_2 by Transition-Metal Doping for Accelerating Hydrogen Evolution Reaction. *J. Am. Chem. Soc.* **2017**, *139*, 15479–15485. [CrossRef]
32. Yu, B.; Chen, Y.; Wang, Z.; Chen, D.; Wang, X.; Zhang, W.; He, J.; He, W. 1T-MoS_2 Nanotubes Wrapped with N-Doped Graphene as Highly-Efficient Absorbent and Eectrocatalyst for Li-S Batteries. *J. Power Sources* **2020**, *447*, 227364. [CrossRef]
33. Long, G.F.; Li, X.H.; Wan, K.; Liang, Z.X.; Piao, J.H.; Tsiakaras, P. Pt/CN-Doped Electrocatalysts: Superior Electrocatalytic Activity for Methanol Oxidation Reaction and Mechanistic Insight into Interfacial Enhancement. *Appl. Catal. B Environ.* **2017**, *203*, 541–548. [CrossRef]
34. Kappera, R.; Voiry, D.; Yalcin, S.E.; Branch, B.; Gupta, G.; Mohite, A.D.; Chhowalla, M. Phase-Engineered Low-Resistance Contacts for Ultrathin MoS_2 Transistors. *Nat. Mater.* **2014**, *13*, 1128–1134. [CrossRef] [PubMed]
35. Xie, Z.; Yu, S.; Ma, X.; Li, K.; Ding, L.; Wang, W.; Cullen, D.A.; Meyer, H.M.; Yu, H.; Tong, J.; et al. MoS_2 Nanosheet Integrated Electrodes with Engineered 1T-2H Phases and Defects for Efficient Hydrogen Production in Practical PEM Electrolysis. *Appl. Catal. B Environ.* **2022**, *313*, 121458. [CrossRef]
36. Zhang, J.; Wang, T.; Pohl, D.; Rellinghaus, B.; Dong, R.; Liu, S.; Zhuang, X.; Feng, X. Interface Engineering of MoS_2/Ni_3S_2 Heterostructures for Highly Enhanced Electrochemical Overall-Water-Splitting Activity. *Angew. Chem. Int. Ed.* **2016**, *55*, 6702–6707. [CrossRef]
37. Wu, Y.; Li, F.; Chen, W.; Xiang, Q.; Ma, Y.; Zhu, H.; Tao, P.; Song, C.; Shang, W.; Deng, T.; et al. Coupling Interface Constructions of MoS_2/$Fe_5Ni_4S_8$ Heterostructures for Efficient Electrochemical Water Splitting. *Adv. Mater.* **2018**, *30*, 1803151. [CrossRef]
38. Wan, K.; Luo, J.; Zhou, C.; Zhang, T.; Arbiol, J.; Lu, X.; Mao, B.W.; Zhang, X.; Fransaer, J. Hierarchical Porous Ni_3S_4 with Enriched High-Valence Ni Sites as a Robust Electrocatalyst for Efficient Oxygen Evolution Reaction. *Adv. Funct. Mater.* **2019**, *29*, 1900315. [CrossRef]
39. Ji, L.; Yan, P.; Zhu, C.; Ma, C.; Wu, W.; Wei, C.; Shen, Y.; Chu, S.; Wang, J.; Du, Y.; et al. One-Pot Synthesis of Porous 1T-Phase MoS_2 Integrated with Single-Atom Cu Doping for Enhancing Electrocatalytic Hydrogen Evolution Reaction. *Appl. Catal. B Environ.* **2019**, *251*, 87–93. [CrossRef]
40. Geng, X.; Sun, W.; Wu, W.; Chen, B.; Al-Hilo, A.; Benamara, M.; Zhu, H.; Watanabe, F.; Cui, J.; Chen, T.P. Pure and Stable Metallic Phase Molybdenum Disulfide Nanosheets for Hydrogen Evolution Reaction. *Nat. Commun.* **2016**, *7*, 10672. [CrossRef]
41. Liu, Q.; Li, X.; He, Q.; Khalil, A.; Liu, D.; Xiang, T.; Wu, X.; Song, L. Gram-Scale Aqueous Synthesis of Stable Few-Layered 1T-MoS_2: Applications for Visible-Light-Driven Photocatalytic Hydrogen Evolution. *Small* **2015**, *11*, 5556–5564. [CrossRef] [PubMed]
42. Liang, Z.; Ahn, H.S.; Bard, A.J. A Study of the Mechanism of the Hydrogen Evolution Reaction on Nickel by Surface Interrogation Scanning Electrochemical Microscopy. *J. Am. Chem. Soc.* **2017**, *139*, 4854–4858. [CrossRef] [PubMed]
43. Li, R.; Liang, J.; Li, T.; Yue, L.; Liu, Q.; Luo, Y.; Hamdy, M.S.; Sun, Y.; Sun, X. Recent Advances in MoS_2-Based Materials for Electrocatalysis. *Chem. Commun.* **2022**, *58*, 2259–2278. [CrossRef] [PubMed]
44. Li, P.; Zhao, G.; Cui, P.; Cheng, N.; Lao, M.; Xu, X.; Dou, S.X.; Sun, W. Nickel Single Atom-Decorated Carbon Nanosheets as Multifunctional Electrocatalyst Supports Toward Efficient Alkaline Hydrogen Evolution. *Nano Energy* **2021**, *83*, 105850. [CrossRef]

45. Takahashi, Y.; Kobayashi, Y.; Wang, Z.; Ito, Y.; Ota, M.; Ida, H.; Kumatani, A.; Miyazawa, K.; Fujita, T.; Shiku, H. High-Resolution Electrochemical Mapping of the Hydrogen Evolution Reaction on Transition-Metal Dichalcogenide Nanosheets. *Angew. Chem. Int. Ed.* **2020**, *132*, 3629–3636. [CrossRef]
46. Meng, X.; Ma, C.; Jiang, L.; Si, R.; Meng, X.; Tu, Y.; Yu, L.; Bao, X.; Deng, D. Distance Synergy of MoS_2-Confined Rhodium Atoms for Highly Efficient Hydrogen Evolution. *Angew. Chem. Int. Ed.* **2020**, *59*, 10502–10507. [CrossRef]
47. Gao, G.; Sun, Q.; Du, A. Activating Catalytic Inert Basal Plane of Molybdenum Disulfide to Optimize Hydrogen Evolution Activity via Defect Doping and Strain Engineering. *J. Phys. Chem. C* **2016**, *120*, 16761–16766. [CrossRef]
48. Liu, M.; Wang, J.A.; Klysubun, W.; Wang, G.G.; Sattayaporn, S.; Li, F.; Cai, Y.W.; Zhang, F.; Yu, J.; Yang, Y. Interfacial Electronic Structure Engineering on Molybdenum Sulfide for Robust Dual-pH Hydrogen Evolution. *Nat. Commun.* **2021**, *12*, 5260. [CrossRef]
49. Gao, S.; Lin, Y.; Jiao, X.; Sun, Y.; Luo, Q.; Zhang, W.; Li, D.; Yang, J.; Xie, Y. Partially oxidized atomic cobalt layers for carbon dioxide electroreduction to liquid fuel. *Nature* **2016**, *529*, 68–71. [CrossRef]
50. Yin, Y.; Han, J.; Zhang, Y.; Zhang, X.; Xu, P.; Yuan, Q.; Samad, L.; Wang, X.; Wang, Y.; Zhang, Z.; et al. Contributions of Phase, Sulfur Vacancies, and Edges to the Hydrogen Evolution Reaction Catalytic Activity of Porous Molybdenum Disulfide Nanosheets. *J. Am. Chem. Soc.* **2016**, *138*, 7965–7972. [CrossRef]
51. Hu, J.; Zhang, C.; Jiang, L.; Lin, H.; An, Y.; Zhou, D.; Leung, M.K.; Yang, S. Nanohybridization of MoS_2 with Layered Double Hydroxides Efficiently Synergizes the Hydrogen Evolution in Alkaline Media. *Joule* **2017**, *1*, 383–393. [CrossRef]
52. Zang, Y.; Niu, S.; Wu, Y.; Zheng, X.; Cai, J.; Ye, J.; Xie, Y.; Liu, Y.; Zhou, J.; Zhu, J.; et al. Tuning orbital orientation endows molybdenum disulfide with exceptional alkaline hydrogen evolution capability. *Nat. Commun.* **2019**, *10*, 1217. [CrossRef] [PubMed]
53. Hou, J.; Zhang, B.; Li, Z.; Cao, S.; Sun, Y.; Wu, Y.; Gao, Z.; Sun, L. Vertically Aligned Oxygenated-CoS_2–MoS_2 Heteronanosheet Architecture from Polyoxometalate for Efficient and Stable Overall Water Splitting. *ACS Catal.* **2018**, *8*, 4612–4621. [CrossRef]
54. Wu, W.; Niu, C.; Wei, C.; Jia, Y.; Li, C.; Xu, Q. Activation of MoS_2 Basal Planes for Hydrogen Evolution by Zinc. *Angew. Chem. Int. Ed.* **2019**, *58*, 2029–2033. [CrossRef]
55. Yang, Y.; Yao, H.; Yu, Z.; Islam, S.M.; He, H.; Yuan, M.; Yue, Y.; Xu, K.; Hao, W.; Sun, G.; et al. Hierarchical Nanoassembly of $MoS_2/Co_9S_8/Ni_3S_2/Ni$ as a Highly Efficient Electrocatalyst for Overall Water Splitting in a Wide pH Range. *J. Am. Chem. Soc.* **2019**, *141*, 10417–10430. [CrossRef]
56. Xu, Q.; Liu, Y.; Jiang, H.; Hu, Y.; Liu, H.; Li, C. Unsaturated Sulfur Edge Engineering of Strongly Coupled MoS_2 Nanosheet-Carbon Macroporous Hybrid Catalyst for Enhanced Hydrogen Generation. *Adv. Energy Mater.* **2019**, *9*, 1802553. [CrossRef]
57. Xu, X.; Zhong, W.; Zhang, L.; Liu, G.; Du, Y. MoS2/NiS Heterostructure Grown on Nickel Foam as Highly Efficient Bifunctional Electrocatalyst for Overall Water Splitting. *Int. J. Hydrogen Energy* **2020**, *45*, 17329–17338. [CrossRef]
58. Jiang, H.; Zhang, K.; Li, W.; Cui, Z.; He, S.A.; Zhao, S.; Li, J.; He, G.; Shearing, P.R.; Brett, D.J.L. MoS_2/NiS Core-Shell Structures for Improved Electrocatalytic Process of Hydrogen Evolution. *J. Power Sources* **2020**, *472*, 228497. [CrossRef]
59. Gaur, A.P.; Zhang, B.; Lui, Y.H.; Tang, X.; Hu, S. Morphologically tailored nano-structured MoS_2 catalysts via introduction of Ni and Co ions for enhanced HER activity. *Appl. Surf. Sci.* **2020**, *516*, 146094. [CrossRef]
60. Kim, M.; Anjum, M.A.R.; Choi, M.; Jeong, H.Y.; Choi, S.H.; Park, N.; Lee, J.S. Covalent 0D-2D Heterostructuring of Co_9S_8-MoS_2 for Enhanced Hydrogen Evolution in All pH Electrolytes. *Adv. Funct. Mater.* **2020**, *30*, 2002536. [CrossRef]
61. Duan, H.; Wang, C.; Li, G.; Tan, H.; Hu, W.; Cai, L.; Liu, W.; Li, N.; Ji, Q.; Wang, Y.; et al. Single-Atom-Layer Catalysis in a MoS_2 Monolayer Activated by Long-Range Ferromagnetism for the Hydrogen Evolution Reaction: Beyond Single-Atom Catalysis. *Angew. Chem. Int. Ed.* **2021**, *60*, 7251–7258. [CrossRef]
62. Qin, J.; Xi, C.; Zhang, R.; Liu, T.; Zou, P.; Wu, D.; Guo, Q.; Mao, J.; Xin, H.; Yang, J. Activating Edge-Mo of 2H-MoS_2 via Coordination with Pyridinic N–C for pH-Universal Hydrogen Evolution Electrocatalysis. *ACS Catal.* **2021**, *11*, 4486–4497. [CrossRef]
63. Zhao, M. One Step Hydrothermal Synthesis of Ni-MoS_2-RGO Bifunctional Electrocatalysts for HER and OER. *Int. J. Electrochem. Sci.* **2021**, *16*, 210323. [CrossRef]
64. Vedhanarayanan, B.; Shi, J.; Lin, J.Y.; Yun, S.; Lin, T.W. Enhanced Activity and Stability of MoS_2 through Enriching 1T-Phase by Covalent Functionalization for Energy Conversion Applications. *Chem. Eng. J.* **2021**, *403*, 126318. [CrossRef]